Title
X-ray diffraction studies of stripelike ferroelectric domains in thin films of BiFeO3

Journal
Physical Review B, 89(21)

ISSN
2469-9950

Authors
Lee, JCT
Damodaran, AR
Ramesh, R
et al.

Publication Date
2014-06-01

DOI
10.1103/physrevb.89.214104

Peer reviewed

X-ray diffraction studies of stripelike ferroelectric domains in thin films of $BiFeO_3$

J. C. T Lee,[1,*] A. R. Damodaran,[2,1] R. Ramesh,[3] L. W. Martin,[2,1] and P. Abbamonte[4,1]
[1]*Materials Research Laboratory, University of Illinois, Urbana, Illinois 61801, USA*
[2]*Department of Materials Science and Engineering, University of Illinois, Urbana, Illinois 61801, USA*
[3]*Department of Materials Science and Engineering, University of California, Berkeley, California 94720, USA*
[4]*Department of Physics, University of Illinois, Urbana, Illinois 61801, USA*
(Received 27 November 2013; revised manuscript received 6 May 2014; published 6 June 2014)

We have used x-ray diffraction to study the structure of strained, epitaxial $BiFeO_3$ (BFO) films, which exhibit ordered arrays of stripelike ferroelectric domains, in which the polarization vector **P** alternates by either 109° or 71°. Diffraction maps exhibit an intricate satellite structure that arises from coherent, gratinglike diffraction from the domain structure. In the case of the 109° arrays, the domain structure was found to exert a strain modulation on the $DyScO_3$ substrate, with the same periodicity, indicating that domains in BFO can have an influence on the substrate structure. In the case of the 71° arrays, in which there is no contrast between neighboring domains and coherent scattering is not expected, weak scattering is nonetheless observed, which we interpret as evidence for previously unobserved, internal strains in these domain walls. To understand the x-ray data, we introduce a simple, single-scattering model that incorporates Gaussian disorder and fits the diffraction maps, providing domain periods and surface "puckering" angles that are in good agreement with atomic force microscopy and piezoresponse force microscopy measurements. Our study demonstrates a simple, computationally inexpensive technique for semiquantitatively interpreting coherent domain scattering in ferroelectric films, and suggests that tuning domain structures is a potential route to engineering the near-surface properties of perovskite oxides.

DOI: 10.1103/PhysRevB.89.214104 PACS number(s): 61.05.cf, 68.55.at

I. INTRODUCTION

One of the defining properties of a ferroelectric material is that it undergoes a reduction in crystal symmetry upon cooling through its Curie temperature. Such a lowering of symmetry allows for the possibility of forming domain walls, i.e., between regions with different ferroelectric order. For example, in $BiFeO_3$ (BFO)—one of the most widely studied ferroelectrics in recent years—the symmetry lowers from cubic to rhombohedral, space group R_{3c}, allowing for the possibility of domain walls across which the polarization vector rotates by 71°, 109°, or 180° [1].

It is now widely established that modifying the degree of substrate strain can be an effective strategy for tuning the properties of ferroelectric thin films [2]. One possible influence of strain can be to enforce the formation of domains: When a ferroelectric film is grown on a substrate with an epitaxial, lattice mismatch, the film may accommodate this strain by forming domain structures, in which the mean in-plane lattice parameter is fine tuned by subtle differences in bond lengths at the domain boundaries. Using substrate strain and control of electrostatic boundary conditions, it was recently shown that it is possible to controllably create periodic domain structures exhibiting monodisperse, 109° or 71° domain walls [3].

Such domain arrays are known to have important consequences for material electronic properties. Such a domain structure was shown, for example, to influence the size of the exchange bias effect in BFO interfaced to a $Co_{0.9}Fe_{0.1}$ ferromagnet [4]. Moreover, domain arrays have been observed to exhibit anomalous conduction properties [5,6]. Broadly speaking, the spontaneous lattice distortions inherent in domain walls can influence band properties or, if strong correlations are present, can cause small changes in Hubbard parameters such as the hopping, on-site Coulomb repulsion, and spin exchange, potentially giving rise to new ground states that are not present in the bulk material. It is therefore crucial to carry out detailed studies capable of characterizing the structural properties of these domain arrays, with atomic-level detail.

X-ray diffraction (XRD) is a widely used technique for studying the structural properties of thin films, especially lattice strain associated with spontaneous distortions, being able to probe features with length scales on the order of the lattice parameter or smaller. Several groups have previously used XRD to probe the structure of BFO thin films exhibiting ferroelectric domain structures. Folkman *et al.* [7,8] studied the domain structures of films exhibiting 109° domain walls (DWs) on a variety of substrates, to understand the influence of epitaxial strain and substrate miscut on the domains and domain walls. Daumont *et al.* [9] also used XRD to study the domain structure and unit cell of 71° DW films on $SrTiO_3$ substrates.

To explain their XRD data, both groups interpreted their results in terms of incoherent scattering from independent domains with symmetry-equivalent unit cells but different crystallographic orientation. In doing so, they were able to characterize the strain-induced changes to the point-group symmetry of the BFO unit cell and its corresponding lattice parameters. However, their approach fails to account for the possibility of coherent scattering from the periodic domain structure itself, which might produce gratinglike features in XRD reciprocal space maps, residing at in-plane momenta determined by the domain periodicity. Such effects have been observed previously in manganite films [10], so there is a great need for a simplified approach to interpreting XRD data from ferroelectric films, which properly accounts for these effects.

*jameslee@lbl.gov

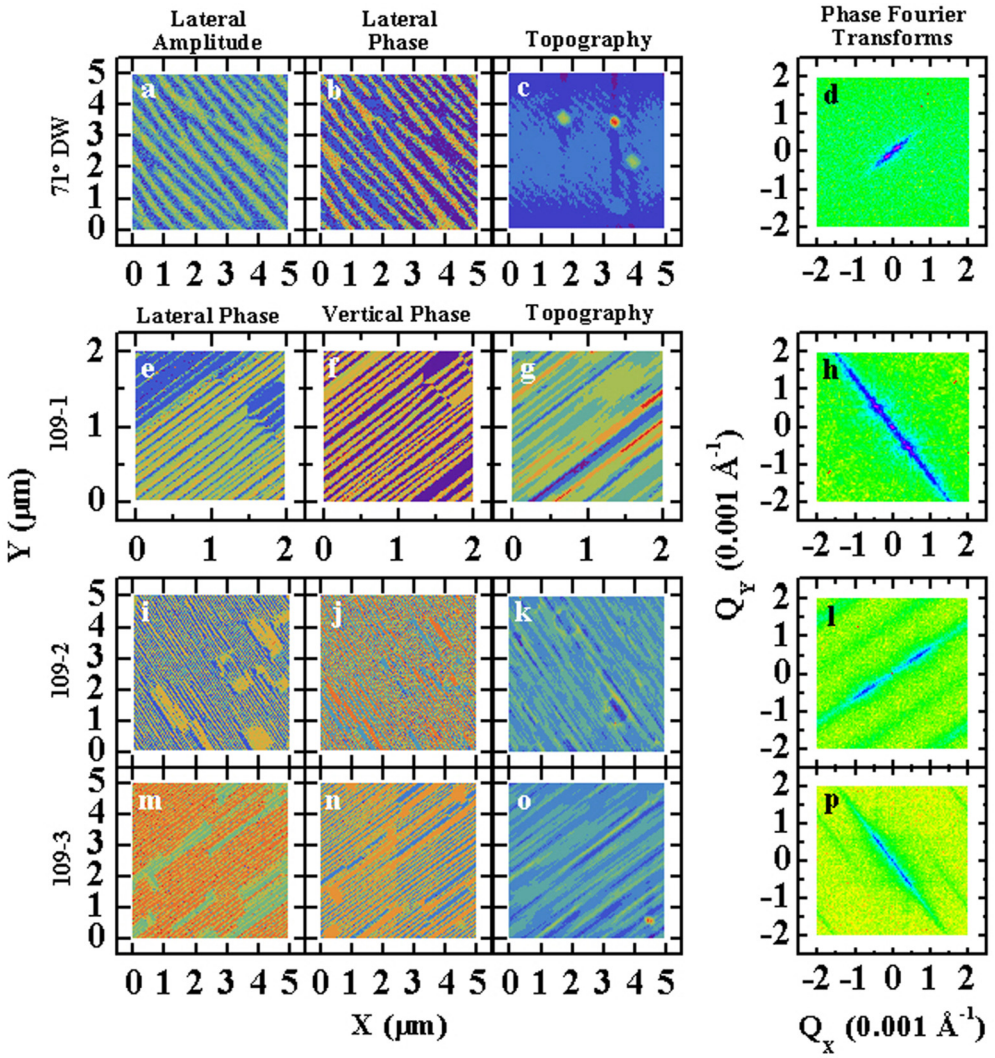

FIG. 1. (Color online) Real-space PFM data and Fourier transforms of the PFM phase data. From left to right: the first and second columns show PFM data, the third column shows topographical maps of the films, and the last column shows Fourier transforms of the data in the second column. Notice that the PFM scans in parts (e) and (f) are shifted with respect to each other by 0.5 μm.

Here, we present an XRD study of BFO thin films that exhibit periodic, monodisperse, stripelike arrays of 109° or 71° domain walls. We present a simple, single-scattering model for interpreting reciprocal space maps that properly accounts for both the crystallographic orientation of the domains and coherent, gratinglike scattering from the periodic domain structure itself. This approach allows, for example, simultaneous determination of both the bond angles and the periodicity of the domain structure, which is in good agreement with piezoresponse force microscopy (PFM), from reciprocal space maps around just a single Bragg peak.

II. PFM AND TOPOGRAPHY

We studied three thin-film arrays of 109° DWs, which we refer to here as 109-1, 109-2, and 109-3, and one film with 71° DWs. The films were grown using pulsed laser deposition, as described by Chu *et al.* [3], on (110)-oriented $DyScO_3$ substrates with small miscut angles.

The arrays of stripelike ferroelectric domains in the films were characterized using PFM [11]. A Cypher atomic force microscope (Asylum Research), with Cr/Pt cantilever tips, was used, which allowed both the amplitude and the phase response to be resolved into "lateral" and "vertical" (normal to the film surface) channels, allowing determination of both the in-plane and out-of-plane components of the ferroelectric polarization **P**. The spatial resolution of the instrument was 30–35 nm, which cannot reveal atomic details but is adequate for probing the coarse domain structure.

The real-space PFM data are shown in Fig. 1. For comparison to the underlying structure, topographic data is also shown. These images exhibit stripelike features that correspond to the periodic, ferroelectric domains. The lateral amplitude and phase data from the 71° DW film are shown in Figs. 1(a) and 1(b). Data from the vertical channels (not shown) are featureless. The fact that only the lateral data show contrast is consistent with previous studies of 71° DWs, in which only the in-plane component of **P** was found to switch between adjacent domains [3].

Both the in-plane and out-of-plane components of **P** should switch directions across a 109° DW. This is most

TABLE I. Characteristic domain structure parameters and lattice spacings of the BFO films. From top row to bottom row: the periods of the ferroelectric domain structures of each film obtained from Fourier transforms of their PFM data, with errors set by the full width at half maximum of the Fourier peak; the lattice parameters associated with the observed BFO (0, 0, 1) Bragg peaks; and, as obtained from fits of the single-scattering model to the x-ray data, as described in Sec. III B, the c-axis tilt angles α of the domains, the domain d spacing, and the Gaussian broadening σ, used in the fits.

(Å)	109-1	109-2	109-3	71°
Ferroelectric domain period	1140.2 ± 283.9	1013.0 ± 349.9	1210.1 ± 230.4	2971.1 ± 575.8
Lattice parameter (c)	3.9675	3.9849	3.9863	3.9641
α (°)	0.608	0.611	0.560	n/a
d (Å)	849.0	763.2	1016.9	1654.5
σ (10^{-3} Å^{-1})	1.98	2.25	1.98	0.44

clearly seen in the lateral [Figs. 1(e), 1(i), 1(m)] and vertical [Figs. 1(f), 1(j), 1(n)] phase data, which both exhibit strong contrast. Defects in the ferroelectric domain structure are also visible: There are patches of film in which the direction of **P** is reversed with respect to the surrounding film, such as that on the right side of Figs. 1(e) and 1(f). If these scans are representative of the whole film, then these defective patches comprise 10–30% of the area of the 109° DW films.

The 71° sample also displays faintly visible vicinal steps due to the substrate miscut [Fig. 1(c)]. More importantly, the surfaces of all the 109° DW samples show stripelike features in the scans [Figs. 1(g), 1(k), 1(o)], which signify a "puckering" of the surface, as was observed in previous atomic force microscopy (AFM) measurements [3]. This puckering is required by symmetry for this particular domain structure to meet the epitaxial condition with the substrate [1].

To reveal the characteristic length scales of the domain structures in the BFO films, Fourier transforms (FTs) of the phase response signal are also displayed in Fig. 1. Transforms of the lateral phase data for the 71° DW film are plotted in Fig. 1(d); transforms of the vertical phase data from the 109° DW films are plotted in Figs. 1(h), 1(l), and 1(p). The blue-violet colored features next to the central peaks are due to the periodic ferroelectric domain structure; the momentum position of these features reveals the average domain period. Notice that the peaks lie along a line perpendicular to the domains.

Determining the average ferroelectric domain period from these FTs requires some prior knowledge of the domain-wall geometry. In the 109° case, the DWs are oriented vertically, i.e., 90° from the surface normal, while the 71° DWs are nominally tilted by 45° [1,3]. The apparent ferroelectric domain period in PFM scans, then, is longer than the true period by a factor of $\sqrt{2}$. The average periods associated with the ferroelectric domain arrays are listed in Table I, with the factor of $\sqrt{2}$ divided out for the 71° DW case.

III. X-RAY DIFFRACTION

In this paper, we confine our observations to reflections near the (0, 0, 1) Bragg peak. While higher-order reflections were accessible, the wealth of scattering features near this peak provided sufficient information to study the domain structure.

To acquire atomic-scale information about the structure of these arrays, we performed XRD measurements using an X'Pert MRD system (PANalytical B. V.), using an incident beam of Cu Kα_1 x rays ($\lambda = 1.5406$ Å) with bandwidth $\Delta\lambda/\lambda = 5 \times 10^{-5}$ and an angular divergence of 30 arc seconds. A line detector with 255 pixels subtending 2.50° recorded the scattered x rays. A primary beam mask shaped the incident beam so that it was five pixels wide on the line detector (or 1/32° across). To observe reflections from the BFO film, we adjusted the detector angle η and the sample tilt θ of the diffractometer. In this paper, Z will denote the direction normal to the film surface, and X will denote the modulation direction of the domain structure. When $\theta = 0$, X is parallel to the incident beam; when $\theta = \eta/2$, the momentum transfer is parallel to Z.

The large size of the domains makes it important to consider the shape of the momentum resolution of the instrument. We will first describe the resolution function at (0, 0, 1). The resolution function is determined by the bandwidth of the incident beam, its angular divergence, the size of the detector pixels, which sets the range of scattered wave vectors that are detected, and the scattering geometry. The bandwidth creates an approximately Gaussian broadening in the direction parallel to the momentum transfer, **Q**, with a standard deviation of 8.65×10^{-5} Å^{-1}. The finite beam divergence broadens the resolution function by 2.52×10^{-4} Å^{-1} along a line tilted counterclockwise from **Q** in the Q_X/Q_Z plane by an angle $\eta/2$, where η is the scattering angle. The finite pixel size broadens the resolution, by an amount 2.22×10^{-3} Å^{-1}, along a line tilted *clockwise* in the Q_X/Q_Z plane by angle $\eta/2$. Accounting for all of these effects, the resulting resolution function is illustrated in Fig. 2(f), which displays a contour representing the half maximum of the resolution function.

This paper focuses on reflections from the domain arrays near the (0, 0, 1) peak. For these reflections, η and θ do not significantly deviate from the angles for (0, 0, 1). Thus, the same resolution function can be used to approximate the resolution at the domain array reflections.

A. 109° DW samples

The diffraction data from the 109° DWs is shown in Figs. 2(a)–2(c). All data sets show a strong (1, 1, 0) Bragg peak from the $DyScO_3$ (DSO) substrate, seen at $Q_Z \sim 1.5936$ Å^{-1}. A streaklike artifact intersects the DSO (1, 1,

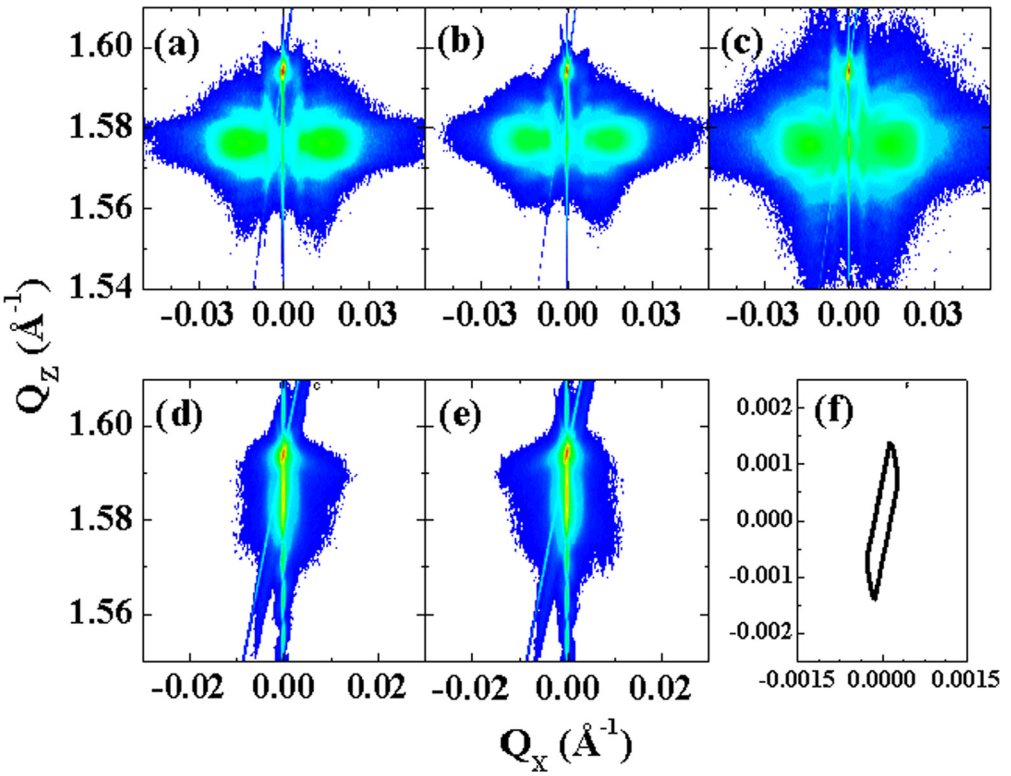

FIG. 2. (Color online) X-ray diffraction data and the resolution function near the (0, 0, 1) peak. The data is plotted in Q_X, the component of the momentum transfer perpendicular to the domain walls, and Q_Z, the component perpendicular to the film surface. (a)–(c) Data from 109-1, 109-2, and 109-3, respectively. (d),(e) Data from the 71° DW film at azimuthal angles that differ by 180°. (f) A contour of constant value of the resolution function.

0) peak and forms a rod of intensity tilted from the (0, 0, L) direction by an angle $\eta/2$ in momentum space. This feature is a saturation effect caused by anomalous broadening of the detector point spread function under conditions of high intensity, and is not related to the sample structure.

A rod of scattering centered on $Q_X = 0$ can be seen that passes through the DSO (1, 1, 0) peak and exhibits an intensity maximum at the expected location of the (0, 0, 1) BFO Bragg peak. The BFO pseudocubic lattice parameter can be extracted from the position of this maximum. Sample-specific lattice parameters are given in the second data row of Table I. This rod itself arises from the finite thickness of the film, which in the ideal case would exhibit Kiessig fringes whose periodicity reflects the thickness of the film. However, in the present case, the surface is corrugated by the puckering effect discussed earlier, which washes out the fringes [3]. Though there is no convenient way to infer film thickness for the 109° DW samples by diffraction, the nominal thickness set during film growth was 1000 Å.

Beside the $Q_X = 0$ rod of scattering, two broad peaks can be seen, roughly centered on ($\pm$ 0.015 Å^{-1}, 0, 1.575 Å^{-1}), which are due to the domain structure, which causes the (0, 0, 1) planes of the domains to have alternating canting angles from one domain to the next (i.e., "puckering").

Some internal structure is visible in these broad peaks. Weak, vertically elongated features are visible [Figs. 2(a)–2(c)] at approximately $Q_X \sim \pm 0.0056$ Å^{-1}. The origin of these features can be determined by comparing the diffraction maps to the Fourier transforms of the PFM data, as shown in Fig. 3. The inner diffraction sidebands and the peaks

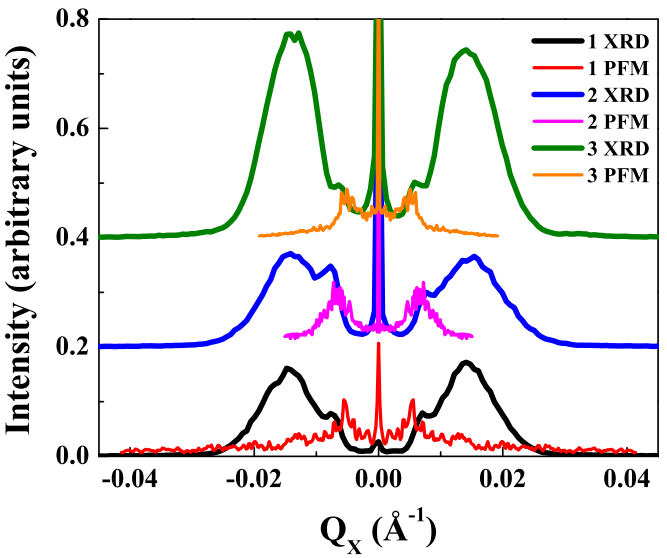

FIG. 3. (Color online) Diffraction data taken along line cuts at $Q_Z = 1.575$ Å^{-1} from 109-1, 109-2, and 109-3 are compared to line cuts taken from the PFM Fourier transforms that intersect both Fourier peaks.

due to the domain period seen in the Fourier transforms coincide in momentum space. This indicates that these diffraction features are due to coherent scattering from the ferroelectric domain structure itself. We will show below that the average domain period d can be deduced from these diffraction sidebands.

Surprisingly, we also observed these features near the DSO (1,1,0) peaks in the 109° DW samples. These satellites are seen in all three of the 109° DW samples, though most prominently in 109-3 (Fig. 2). In 109-3, the pronounced satellite peaks appear at the same Q_Z as the substrate peak. This observation and the Q_X positions of the satellites indicate that these features are due to the thin-film domain structure, which is causing a modulation of the substrate structure. This effect demonstrates that it is possible for domain structures in ferroelectric films to exert influence on the structure of the substrate.

B. Single-scattering model

We now show that it is possible to explain the essential features of the data just discussed using a simple, single-scattering model of the charge density, illustrated in Fig. 4(a). In our model, the average charge density of the film is the same for all domains. The contrast mechanism giving rise to coherent scattering between the ferroelectric domain structure and the Bragg peaks of the domains is the alternating sign of the c-axis canting angles between adjacent domains.

The only observable Bragg reflection from BFO in Fig. 2 is the (0,0,1). For this reason, we can replace the full structure of the BFO unit cell with a sinusoidal function whose amplitude represents a single Fourier component of the electron density, and whose period is equal to the c-axis lattice parameter.

The domains are treated as rectangular slabs of infinite extent along the z axis, with widths along the x axis that are half the ferroelectric domain period. Pairs of these slabs form the motifs that repeat throughout the film [see Fig. 4(a)]. The period of the resulting domain pattern is used as a parameter that can be varied to fit the diffraction data of each 109° DW film. The domain walls are not given any internal structure; instead, they are treated as step functions that act as sharp edges to the domains.

Since adjacent domains are distinguished by the alternating sign of their (0,0,1) plane canting angles, the basic repeating unit is a pair of adjacent ferroelectric domains with c-axis directions that are mirror reflected through the Y-Z plane. This unit cell is illustrated in Fig. 4. The c-axis modulation wave vectors for each canted domain lie in the X-Z plane: $\mathbf{k}_R = 2\pi[\hat{\mathbf{x}}\sin(\alpha) + \hat{\mathbf{z}}\cos(\alpha)]/c$ and $\mathbf{k}_L = 2\pi[-\hat{\mathbf{x}}\sin(\alpha) + \hat{\mathbf{z}}\cos(\alpha)]/c$, where c is the pseudocubic lattice parameter and α is the domain canting angle. The subscripts "L" and "R" denote the direction in which the c axis of each domain points (Fig. 4). The canting angle was estimated to be $\alpha \sim 0.34°$ from AFM measurements by Chu *et al.* [3]. Here, we treat α as a fit parameter to model the diffraction data.

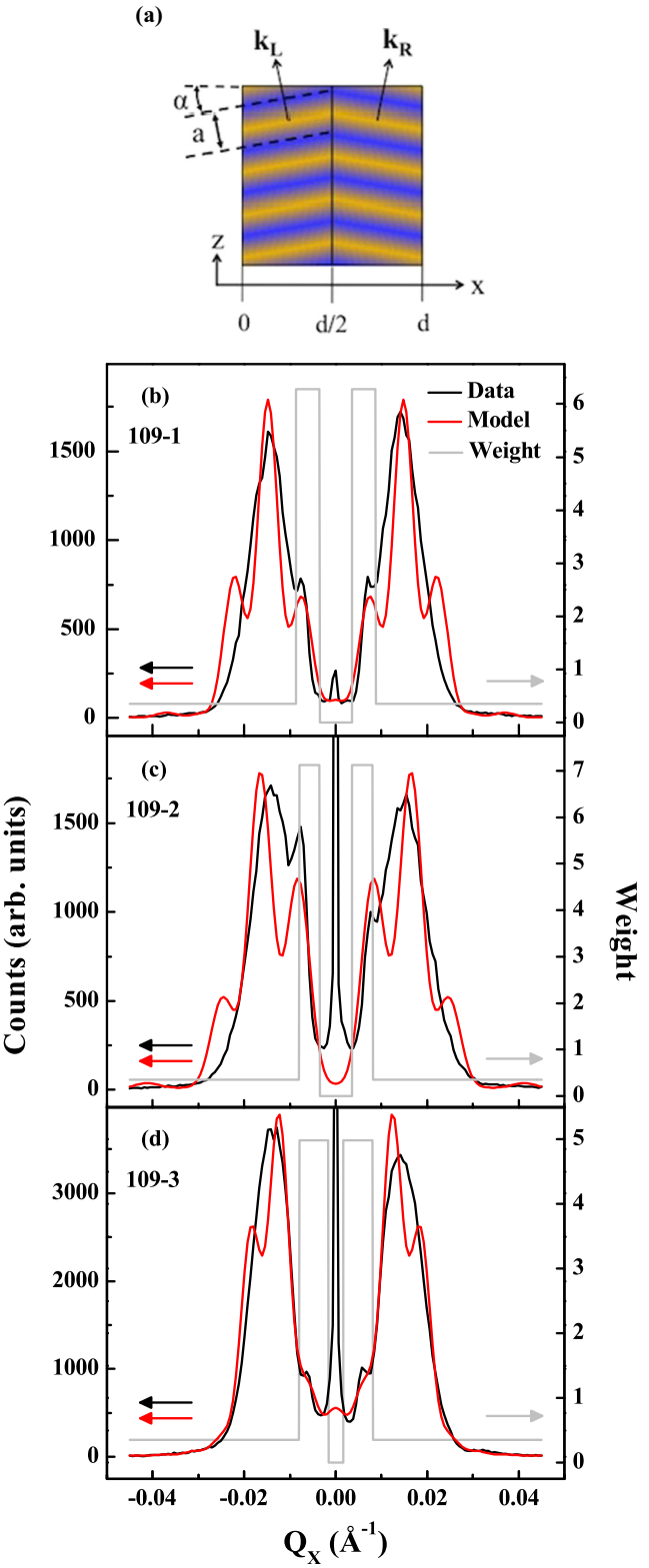

FIG. 4. (Color online) (a) Model unit cell for the 109° DW system. The blue and yellow pattern represents the modulation of the average charge density due to the canted (001) planes. Reciprocal space vectors $\mathbf{k}_L$ and $\mathbf{k}_R$ are associated with the c-axis planes, with lattice spacing a; the canting angle is α. The unit cell width is d. (b)–(d) Fits to 109° DW x-ray data using Gaussian broadened model structure factors based on Eq. (2). The weight function used in the fits is also shown.

In terms of these parameters, the real-space charge density for a single, repeating unit is

$$\begin{aligned}\rho_{\text{cell}} &= \rho_0\Bigg[\cos(\mathbf{k}_{\text{R}}\cdot\mathbf{r})\Theta(x)\Theta\left(\frac{d}{2}-x\right)\\ &\quad+\cos(\mathbf{k}_{\text{L}}\cdot\mathbf{r})\Theta(-x)\Theta\left(x+\frac{d}{2}\right)\Bigg]\\ &= \rho_0\Bigg[\cos\left\{\frac{2\pi}{c}[x\sin(\alpha)+z\cos(\alpha)]\right\}\Theta(x)\Theta\left(\frac{d}{2}-x\right)\\ &\quad+\cos\left\{\frac{2\pi}{c}[z\cos(\alpha)-x\sin(\alpha)]\right\}\Theta(-x)\Theta\left(x+\frac{d}{2}\right)\Bigg].\end{aligned} \tag{1}$$

Here, ρ_0 is the amplitude of the (0,0,1) Fourier component of a BFO unit cell, and d is the ferroelectric domain repeat distance which, like α, will be used as a fit parameter to model the diffraction data. In terms of this repeating unit, the charge density for the complete system is $\rho(x,z)=\sum_{n=-\infty}^{\infty}\rho_{\text{cell}}(x-nd,z)$, with the index n running over all pairs of ferroelectric domains.

The structure factor for this ideal periodic structure, $\rho_{\mathbf{G}}$, is defined as $\rho(\mathbf{r})=\sum_{\mathbf{G}}\rho_{\mathbf{G}}e^{-i\mathbf{G}\cdot\mathbf{r}}$, where $\mathbf{G}=2\pi[H/d,0,\cos(\alpha)/c]$ is a reciprocal lattice vector defined by integer Miller index H. The modulus squared of $\rho_{\mathbf{G}}$ is proportional to the scattered intensity and can be compared to the diffraction patterns [12]. The effects of domain structural disorder, not accounted for in this expression, will be incorporated when comparing to the data.

The structure factor associated with Miller index H can be computed analytically and has the form

$$\begin{aligned}\rho_H &= \frac{\rho_0}{4}i^{\frac{d}{c}\sin(\alpha)}\Bigg\{(-i)^H\frac{\sin\left\{\frac{\pi}{2}\left[\frac{d}{c}\sin(\alpha)-H\right]\right\}}{\frac{\pi}{2}\left[\frac{d}{c}\sin(\alpha)-H\right]}\\ &\quad+i^H\frac{\sin\left\{\frac{\pi}{2}\left[\frac{d}{c}\sin(\alpha)+H\right]\right\}}{\frac{\pi}{2}\left[\frac{d}{c}\sin(\alpha)+H\right]}\Bigg\}.\end{aligned} \tag{2}$$

This result only holds true if the domain walls are oriented normal to the substrate surface; different inclinations of the walls will create different restrictions on where the diffraction can appear, as will be seen in the 71° DW case.

The model structure factor, given by Eq. (2), was compared to the diffraction data from the 109° DW films in order to extract values of the (0,0,1) plane canting angle α and the ferroelectric domain periods. For this comparison, we examined line cuts through the data in the Q_X direction centered on $Q_Z = 1.576$ Å^{-1}, which are plotted in Fig. 4. These line cuts intersect the centers of the broad peaks and the sidebands, so they contain sufficient information to determine the canting angles and ferroelectric domain periods.

To perform an accurate fit, disorder in the domain pattern—which is clearly evident in real-space images in Fig. 2—must be incorporated into our model. While sophisticated, statistical disorder models exist for this purpose [10], for simplicity we will assume that the structure exhibits uncorrelated, Gaussian disorder [13]. In this case, the Bragg reflections are not δ functions, but have the form of Gaussian functions whose integrated intensity is equal to $|\rho_H|$, and whose width σ is a third fit parameter that describes the degree of roughness. The fit results, optimizing all three parameters (α, d, and σ), are shown in Fig. 4 and the fit parameters are listed in Table I. The domain periods are within 25% of the PFM values, and the average canting angle is 0.593°, as compared to ≈0.34° canting angle reported in Chu *et al.* [3]. One reason for the difference may be that XRD measures the canting angle of the bulk crystal structure, while AFM measures that of the surface, which need not be exactly the same.

Features reminiscent of the broad diffraction maxima at $Q_X \sim \pm 0.015$ Å^{-1} are obtained. Making an analogy with diffraction gratings, this shows that the broad peaks arise because the (0, 0, 1) Bragg peaks "blaze" several lower order structure factor components. Features corresponding to the domain structure sidebands seen in the data are also reproduced at approximately the same in-plane momentum positions. To ensure that the fits would account for the sidebands, which are much smaller than the broad peaks, increased weight was placed on the sidebands, as illustrated in Fig. 4. The weight on the data points of the sharp peak centered on $Q_X = 0$ was set to zero as the peak likely arises from a feature other than the ferroelectric domain structure.

C. 71° DW sample

Unlike the 109° DW samples, the 71° DW sample has a smooth surface, due to a lack of domain puckering [3]. Without this puckering, the c-axis planes of the domains are parallel to each other, with no canting angle contrast between them. Hence, one expects to see a single (0, 0, 1) peak in the diffraction map, without domain satellites of the visible sort discussed in Secs. III A and III B. Nonetheless, we will see below that a subtle diffraction effect can be seen that is associated with the domain structure.

XRD data from the 71° DW sample are shown in Figs. 2(d) and 2(e). The data shown in Fig. 2(d) are taken with the sample in a reference 0° position and the data in Fig. 2(e) are taken with the sample rotated about its surface normal by 180°. Just as for the 109° DW samples, a DSO (1, 1, 0) Bragg peak is seen at $Q_Z \approx 1.5936$ Å^{-1}.

Since the surface of the 71° DW sample is smooth, Kiessig fringes are visible in the diffraction along the (0, 0, L) rod of scattering, running through the BFO and DSO Bragg peaks, as is shown in Figs. 2(d) and 2(e). The BFO pseudocubic lattice parameter extracted from the intensity maximum was $c = 3.9641$ Å. A fit to the Kiessig fringes yields a film thickness of 727 ± 26 Å.

While off-specular scattering is not expected, we nevertheless observed diffuse scattering centered on the (0, 0, 1) Bragg peak of BFO [Figs. 2(d) and 2(e)]. This diffuse scattering was observed to reverse direction when the sample is rotated by 180° [Figs. 2(d) and 2(e)], which demonstrates that it is not a resolution effect. As illustrated in Fig. 5, which shows cuts through the (0,0,1) reflection for two orthogonal directions, the diffuse scattering was found to be maximal along a line tilted 45° away from the surface normal. This angle is significant, since the domain walls are known to be tilted 45° from the normal direction. This suggests, surprisingly, that the diffuse scattering arises from the domain structure, similar to the 109° case.

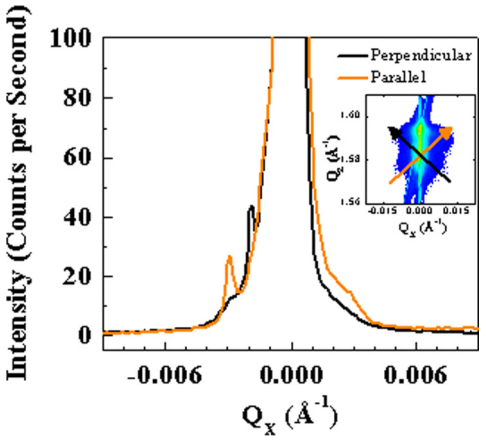

FIG. 5. (Color online) Line cuts from the 0° diffraction data of the 71° sample. The line cut through the diffuse scattering around the (0, 0, 1) Bragg peak (orange) is plotted against a line cut going in a perpendicular direction (black). The orange line cut shows fine structure at $Q_X \approx 0.003$ Å^{-1} that is not seen in the black line cut. Peaks at $Q_X \approx -0.003$ and -0.0015 Å^{-1} are from detector artifacts.

As mentioned earlier, unlike the 109° DW samples, there is no canting angle contrast between the domains in the 71° DW film, since the (001) planes of neighboring ferroelectric domains are parallel. This constraint on the (0,0,1) planes is necessary in order for coherent interfaces to form along the {110} crystallographic planes [1]. Hence, we are led to conclude that there exists some kind of charge density modulation—perhaps a distortion in the unit cell volume or c-axis lattice parameter—associated with the domain walls with a period of $d/2$, i.e., half the ferroelectric domain period.

Without specifying its precise origin, we can model this modulation by superposing a sinusoidal function on top of the underlying crystal structure, as illustrated in Fig. 6(a). The 71° DWs run parallel to the (101) planes so, using the same coordinate system as earlier, the modulation wave vector is $\mathbf{k}_c = 2\pi\hat{\mathbf{z}}/c$ and the domain-wall wave vector is $\mathbf{k}_{DW} = \pi(\hat{\mathbf{x}} - \hat{\mathbf{z}})/d$. Using step functions to define the domains, the charge density of a single domain is given in real space by

$$\begin{aligned}\rho_{\text{cell}} =& \rho[1 + \Delta\cos(\mathbf{k}_{DW}\cdot\mathbf{r})]\cos(\mathbf{k}_c\cdot\mathbf{r}) \\ &\times \Theta(x - z)\Theta(d/\sqrt{2} - x + z) \\ =& \rho\{1 + \Delta\cos[2\sqrt{2}\pi(x - z)/d]\}\cos(2\pi z/c) \\ &\times \Theta(x - z)\Theta(d/\sqrt{2} - x + z), \end{aligned} \tag{3}$$

where $d = 2974.1$ Å is the average ferroelectric domain period seen in PFM scans, and Δ is a dimensionless parameter that characterizes the amplitude of the modulation. It is assumed that the modulation is small, i.e., $\Delta \ll 1$.

As before, the total density of the complete, periodic structure is $\rho(x,z) = \sum_{n=-\infty}^{\infty}\rho_{\text{cell},n}(x - nd/\sqrt{2}, z)$. The reciprocal lattice vectors for this structure are $\mathbf{G} = 2\pi(\sqrt{2}H/d, 0, 1/c - \sqrt{2}H/d)$, where H again is an integer Miller index. The structure factor then has the form

$$\begin{aligned}\rho_H = \frac{\rho}{2}e^{i\pi H}\left(\frac{\sin(\pi H)}{\pi H} - \frac{\Delta}{2}\left\{\frac{\sin[\pi(1-H)]}{\pi(1-H)}\right.\right. \\ \left.\left. + \frac{\sin[\pi(1+H)]}{\pi(1+H)}\right\}\right). \end{aligned} \tag{4}$$

Equation (4) implies the existence of a series of satellite peaks around the (0, 0, 1) Bragg peak of BFO. The first term in Eq. (4) creates a peak at $\mathbf{Q}_0 = 2\pi/c\hat{\mathbf{z}}$, which is the (0, 0, 1) Bragg peak itself. The second and third terms create the satellites, which reside at $\mathbf{Q}_\pm = 2\pi[\pm\sqrt{2}\hat{\mathbf{x}}/d + (1/c \mp \sqrt{2}/d)\hat{\mathbf{z}}]$, i.e., on lines tilted 45° away from the $(0,0,L)$ direction; the sign of the line's

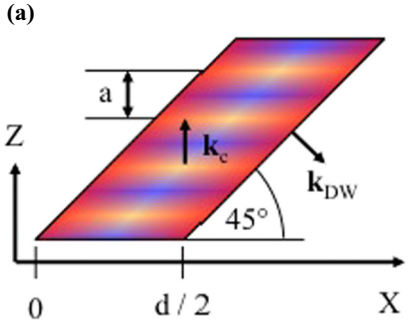

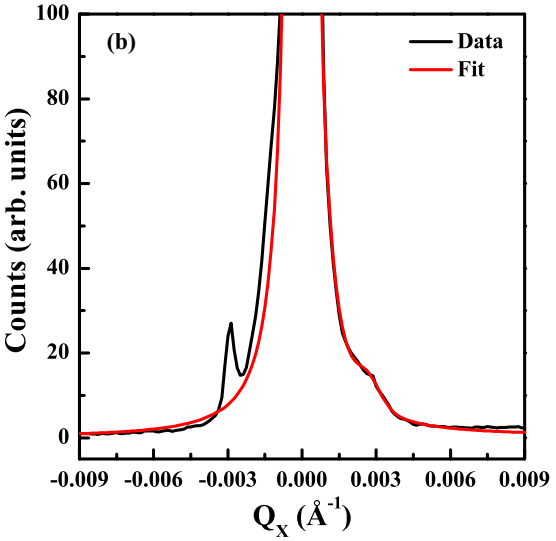

FIG. 6. (Color online) (a) Diagram of the 71° DW system model unit cell. The blue and yellow pattern represents a modulation of the average charge density in the unit cell due to the (001) planes, with lattice spacing a. The associated reciprocal space vector is $\mathbf{k}_c$. The vector $\mathbf{k}_{DW}$ is the wave vector associated with the domain-wall spacing. The red pattern represents a charge density modulation parallel to the domain walls. (b) Simulated 71° DW scattering in the Q_X/Q_Z plane based on Eq. (4).

slope will change if $\mathbf{k}_{\mathrm{DW}}$ points in the other possible direction, $\mathbf{k}_{\mathrm{DW}} = 2\sqrt{2}\pi(\hat{\mathbf{x}} + \hat{\mathbf{z}})/d$.

While the features are not as pronounced as in the 109° DW case, this framework permits a qualitative comparison that provides some understanding of Figs. 2(d) and 2(e). Figure 6 shows a simulated diffraction profile created using a model based on Eq. (4). Parameters for the model were obtained by fits to data such as shown in Fig. (6). Both the shoulderlike peak in the diffuse scattering and the (0, 0, 1) peak were modeled as pseudo-Voigt functions. Just as for the 109° DW case, we assume that the 71° DW structure exhibits uncorrelated, Gaussian disorder causing broadening of the peaks along the direction of $\mathbf{k}_{\mathrm{DW}}$. The detector point spread function streak (i.e., the sharp peak near $Q_X \sim -0.003$ Å) obscures some of the diffuse scattering. In our fits, therefore, we left out that region of the scan and took into account only the central peak, the shoulderlike feature, and the background far away from the central peak.

The fit yielded a central peak that is nearly resolution limited, which is expected for a system of domains with very-well-aligned c axes, and a much smaller and broader harmonic peak near the location of the shoulderlike features. The fit yields a d spacing of 1654.5 Å, as listed in Table I. This places the harmonic peaks seen in the charge density model nearly the same distance away from the BFO (0, 0, 1) in reciprocal space as the shoulderlike features seen in the line scan. The d spacing is also similar to the *domain-wall* period: $d/2 = 1487.0$ Å, as deduced from the PFM data and nominal domain structure.

Comparing the integrated intensities of the (0, 0, 1) peak to the intensity of the shoulder at $Q_X \approx 0.003$ Å^{-1}, the ratio of which is ∼523, we estimate that $|\Delta| = 0.087$. This suggests that the strain or atomic displacements giving rise to the diffuse scattering are at the ∼8.7% level.

IV. DISCUSSION

The success of these domain structure models indicates that one does not necessarily need to resort to detailed analyses of unit cells and atomic positions to capture many of the salient structure features of the system.

However, there are some aspects of the data that these models did not replicate. One such feature is the strong central peak seen in the 109° DW data. Though there is a central peak in the model for $H = 0$, the intensity and sharpness of the observed peak are not accounted for by the canting angle contrast model. This is in part because the substrate peak and its truncation rod are not accounted for in the structure factor, which will run through $Q_X = 0$ and give a small peak such as the one seen in Fig. 4(d). Defects in the sample could also contribute. Having only surveyed 4 and 25 μm^2 patches of film, the possibility that there are regions of the sample that do not exhibit domains, which could contribute to a sharp central peak, cannot be ruled out. Such regions are known to exist in other (0, 0, 1)-oriented BFO films: the nanodiffraction experiments by Hruszkewycz *et al.* [14], on thin films exhibiting 109° DW arrays deposited on $TbScO_3$ substrates, showed many areas of the film that displayed no canting of the c-axis planes.

The data also exhibit asymmetric sidebands, whereas the model yields symmetric scattering. This is not an absorption effect as the asymmetry changes direction if the sample is rotated 180°. One plausible explanation is the change in orientation of the resolution function with sample rotations away from Bragg geometry. The clockwise tilt of the resolution function shown in Fig. 2(f) is that expected when aligned to (0, 0, L). Rotations of the sample away from the Bragg angle cause the resolution function to tilt away from the $Q_X = 0$ line by the sample offset angle. Tilting the sample to either side of the Bragg angle then causes the resolution function to exhibit slightly different tilts for each case, causing it to integrate the intensity from the sidebands in an uneven manner.

There is also a phase ambiguity in the 71° DW charge density model. The density fluctuations were spatially assigned to domain walls in the real-space model. The same result for intensities will be obtained if the sinusoidal modulation of the average charge density is shifted by some phase so that its crests no longer lie on domain walls. The same holds true if charge density modulation amplitude Δ is positive or negative, as either value gives the same scattered intensity. These ambiguities are examples of the classic "phase problem" of XRD. Intuition can help clear up some of the ambiguity: if the charge densities at each domain wall are to be treated as identical, it seems natural to assume that the density modulation in a domain will be symmetric about the center of the domain, though one cannot say for sure if it is the crest or the trough of the modulation that is centered on the wall.

What might be the physical origin of the average charge density modulation in the 71° DW system? One possibility is strain associated with the domain walls. Regions of the film with compressive strain should have a higher average density than bulklike regions, while regions with tensile strain should have a lower-than-bulk average density. For the 71° DW case, a model with an average density modulation parallel to the domain wall successfully reproduces the fine structure seen in the diffuse scattering. It is tempting to connect the average charge density modulation to the modulations of strain normal to the domain walls. This is a reasonable connection to make, as others [15] have calculated in Landau free-energy models film strains at domain walls that vary significantly from bulk values for realistic treatments of several materials.

V. CONCLUSION

In summary, we have shown that a simple charge density model of the domain structure compares in a satisfactory way to data collected around the (0, 0, 1) Bragg peak of BFO. The canting angle contrast model, which accounts for coherent scattering between the canted c-axis planes and the domain structure, successfully captures the essential features of the diffraction data from the 109° DW samples. Values of the canting angles of the (0, 0, 1) planes obtained from fits to the diffraction data compare favorably to the AFM result reported by Chu *et al.* [3]. The domain array periods extracted from the data using the model are also within the error bars of the PFM values of the domain array periods of the samples. For

the 71° DW system, charge density modulations associated with the domain walls successfully reproduce many of the features of the diffuse scattering around (0, 0, 1). Using 45° inclined domain walls in the model, harmonic peaks arise that coincide with faint shoulderlike features seen in line cuts through the diffuse scattering: the d spacing associated with the shoulders is nearly equal to the domain-wall period.

The diffraction data also contains signatures of the substrate strain being modulated due to the formation of a coherent interface between the $DyScO_3$ lattice and the BFO film. This indicates that domain structures might be used to influence the near-surface properties of bulk materials.

ACKNOWLEDGMENTS

The research described here was carried out in part in the Frederick Seitz Materials Research Laboratory Central Facilities, University of Illinois. Funding was provided by the US Department of Energy, Office of Basic Energy Sciences, under Grant No. DE-FG-06-ER 46285.

[1] S. K. Streiffer, C. B. Parker, A. E. Romanov, M. J. Lefevre, L. Zhao, J. S. Speck, W. Pompe, C. M. Foster, and G. R. Bai, J. Appl. Phys. **83**, 2742 (1998).

[2] D. G. Schlom, L.-Q. Chen, C.-B. Eom, K. M. Rabe, S. K. Streiffer, and J.-M. Triscone, Annu. Rev. Mater. Res. **37**, 589 (2007).

[3] Y.-H. Chu, Q. He, C.-H. Yang, P. Yu, L. W. Martin, P. Shafer, and R. Ramesh, Nano Lett. **9**, 1726 (2009).

[4] L. W. Martin, Y.-H. Chu, M. B. Holcomb, M. Huijben, P. Yu, S.-J. Han, S. X. Wang, and R. Ramesh, Nano Lett. **8**, 2050 (2008).

[5] J. Seidel, L. W. Martin, Q. He, and Q. Zhan, Nat. Mater. **8**, 229 (2009).

[6] J. Seidel, P. Maksymovych, Y. Batra, A. Katan, S.-Y. Yang, Q. He, A. P. Baddorf, S. V. Kalinin, C.-H. Yang, J.-C. Yang, Y.-H. Chu, E. K. H. Salje, H. Wormeester, M. Salmeron, and R. Ramesh, Phys. Rev. Lett. **105**, 197603 (2010).

[7] C. M. Folkman, S. H. Baek, H. W. Jang, C. B. Eom, C. T. Nelson, X. Q. Pan, Y. L. Li, L. Q. Chen, A. Kumar, V. Gopalan, and S. K. Streiffer, Appl. Phys. Lett. **94**, 251911 (2009).

[8] C. M. Folkman, S.-H. Baek, and C.-B. Eom, J. Mater. Res. **26**, 2844 (2011).

[9] C. J. M. Daumont, S. Farokhipoor, A. Ferri, J. C. Wojdeł, J. Íñiguez, B. J. Kooi, and B. Noheda, Phys. Rev. B **81**, 144115 (2010).

[10] U. Gebhardt, N. V. Kasper, A. Vigliante, P. Wochner, H. Dosch, F. S. Razavi, and H.-U. Habermeier, Phys. Rev. Lett. **98**, 096101 (2007).

[11] E. Soergel, J. Phys. D **44**, 464003 (2011).

[12] W. H. Zachariasen, *Theory of X-ray Diffraction in Crystals* (Dover, New York, 1967).

[13] S. K. Sinha, E. B. Sirota, S. Garoff, and H. B. Stanley, Phys. Rev. B **38**, 2297 (1988).

[14] S. O. Hruszkewycz, C. M. Folkman, M. J. Highland, M. V. Holt, S. H. Baek, S. K. Streiffer, P. Baldo, C. B. Eom, and P. H. Fuoss, Appl. Phys. Lett. **99**, 232903 (2011).

[15] W. T. Lee, E. K. H. Salje, and U. Bismayer, J. Appl. Phys. **93**, 9890 (2003).